5-15-2003

Mechanisms of photoluminescence from silicon nanocrystals formed by pulsed-laser deposition in argon and oxygen ambient

X. Y. Chen
National University of Singapore

Yongfeng Lu
University of Nebraska-Lincoln, ylu2@unl.edu

Y. H. Wu
National University of Singapore

B. J. Cho
National University of Singapore

M. H. Liu
National University of Singapore

See next page for additional authors

Mechanisms of photoluminescence from silicon nanocrystals formed by pulsed-laser deposition in argon and oxygen ambient

X. Y. Chen
Department of Electrical and Computer Engineering, National University of Singapore, 10 Kent Ridge Crescent, Singapore 119260

Y. F. Lu[a)]
Department of Electrical Engineering, University of Nebraska, Lincoln, Nebraska 68588-0511

Y. H. Wu, B. J. Cho, M. H. Liu, D. Y. Dai, and W. D. Song
Department of Electrical and Computer Engineering, National University of Singapore, 10 Kent Ridge Crescent, Singapore 119260

(Received 2 December 2002; accepted 3 March 2003)

We have investigated the different mechanisms of photoluminescence (PL) of silicon nanocrystals due to the quantum confinement effect (QCE) and interface states. Si nanocrystals were formed by pulsed-laser deposition in inert argon and reactive oxygen gas. The collisions between the ejected species greatly influence the morphology of the Si nanocrystals and cause a transition from a film structure to a porous cauliflowerlike structure, as the ambient gas pressure increases from 1 mTorr to 1 Torr. The oxygen content of the Si nanocrystals increases with increasing O_2 ambient pressure, and nearly SiO_2 stoichiometry is obtained when the O_2 pressure is higher than 100 mTorr. Broad PL spectra are observed from Si nanocrystals. The peak position and intensity of the PL band at 1.8–2.1 eV vary with ambient gas pressure, while intensity changes and blueshifts are observed after oxidation and annealing. The PL band at 2.55 eV shows vibronic structures with periodic spacing of 97 ± 9 meV, while no peak shift is found before and after oxidation and annealing. Raman and transmission electron microscope measurements show consistent results in crystal size while more accurate atomic force microscope measurements reveal a smaller crystal size. X-ray diffraction reveals a polycrystal structure in the Si nanocrystals and the crystallinity improves after annealing. Combined with the PL spectra of Si nanocrystals obtained by crumbling electrochemically etched porous Si layer, the results clearly demonstrate that the PL band at 1.8–2.1 eV is due to the QCE in the Si nanocrystal core, while the PL band at 2.55 eV is related to localized surface states at the SiO_x/Si interface. © *2003 American Institute of Physics.* [DOI: 10.1063/1.1569033]

I. INTRODUCTION

Ever since visible photoluminescence (PL) spectra were observed in silicon nanostructures,[1–3] Si nanocrystals have attracted great interest in the microelectronics, optoelectronics, and biomedical industries, since crystalline (c-)Si is the primary material for microelectronic integrated circuits and is being extensively studied. In a metal-oxide-silicon structure, memory based on a nanocrystal floating gate has shown great promise for future applications in ultradense and ultralow-power flash memory with faster read and write times, higher reliability, and lower power consumption.[4,5] In optoelectronics, the development of Si nanostructured materials for light emitting devices at room temperature has created a new opportunity for incorporating optoelectronic functions into Si integrated circuit technology. The area of Si nanocrystals is currently one of the most active frontiers in physics and chemistry. Si nanocrystals have been synthesized by several techniques, such as microwave- or laser-induced decomposition of silanelike precursors,[2,6] ion implantation of Si^+,[7,8] electrochemical etching of Si wafers,[9,10] and pulsed-laser deposition (PLD) of Si.[11,12] Among them, PLD is one of the most flexible and promising techniques due to its ability to control the size and distribution of nanocrystals and maintain crystal purity in a cold-wall processing ambient.[12] In the PLD method, the size and distribution of Si nanocrystals can be controlled by varying the background gas species and pressure, laser fluence, target-to-substrate distance, and subsequent annealing or oxidation. Impurities can be doped before the formation of nanocrystals. The introduction of ambient gas during PLD is necessary to cool down and condense the ablated material into nanocrystals with the desired sizes. Yoshida *et al.*[13] reported that the size distribution of Si nanocrystals can be controlled from 2 to tens of nanometers by varying the background gas species and pressure. Suzuki *et al.*[14] recommended that PLD plus a low-pressure-differential mobility analyzer and a nozzle jet can get uniform Si nanocrystals with little size deviation. Thus, PLD is thought to be a mature method and is extensively used to form Si nanocrystals.[11–16]

In this work, Si nanocrystals were formed by PLD in inert argon and reactive oxygen gas. Dry oxidation and nitrogen annealing were carried out on the as-deposited Si nanocrystals. The purpose of this work is to study the effects

a)Author to whom correspondence should be addressed; fax: 402-472-4732; electronic mail: yflu@engr.unl.edu

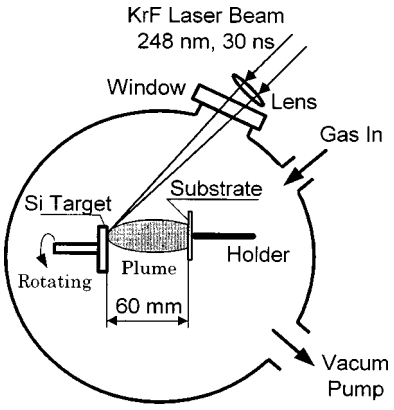

FIG. 1. Schematic of PLD system.

of deposition and thermal treatment conditions on the structures and PL properties of Si nanocrystals.

II. EXPERIMENT

The PLD system utilized is schematically shown in Fig. 1. The laser beam was directed by a mirror and then focused by a quartz lens (50 cm focal length) onto the target at an incident angle of 45°. After laser ablation of the Si powder target, a luminescent Si plasma plume perpendicular to the target surface was generated and expanded toward the substrates, which were identical to the target. The hot ejected species (atoms, ions, clusters with a few atoms) in the plume were cooled down and condensed into nanocrystals in ambient gas and deposited on Si(100) substrates. A pulsed KrF excimer laser (Lambda Physik LPX 100, $\lambda = 248$ nm, $\tau = 30$ ns) was used as light source. The laser fluence was set at 3.0 J/cm^2 and the repetition rate was 10 Hz. The Si target was rotated constantly by an external motor to provide each pulse with a fresh surface. The substrates were cleaned with acetone and ethanol ultrasonic baths before deposition. The substrates were not heated or cooled during deposition. The target-to-substrate distance was approximately 6 cm. After the base vacuum was pumped down to 1.0×10^{-5} Torr, Ar (purity 99.999%) or O_2 (purity 99.7%) gas was introduced into the vacuum chamber and maintained at a constant pressure during deposition. The deposition time was 60 min.

In a luminescent Si plasma plume, large clusters move at a smaller angle from target to substrate compared with small clusters, due to scattering by the ambient gas. Roughly speaking, large crystals are formed in the center of the plume, while smaller ones are formed near the plume edge. Thus, larger nanocrystals are deposited on the substrates which are near the plume center. In this work, all the samples were obtained at the plume center axis for consistency.

After deposition, dry oxidation was carried out on the as-deposited Si nanocrystals in constant O_2 gas flow for 180 min at a temperature of either 900 or 700 °C. Annealing was also applied to the as-deposited Si nanocrystals in constant N_2 (purity 99.9995%) gas flow for 60 min at a temperature of 1100 °C.

The deposited Si nanocrystals were characterized by several methods. The surface morphology was observed using a Hitachi S-4100 field-emission scanning electron microscope. The composition was determined by x-ray photoelectron spectroscopy (XPS) with a Physical Electronics Quantum 2000 Scanning ESCA microprobe. The PL and Raman spectra were recorded by PL and Raman spectroscopy (Renishaw Raman microscope) with an electrically cooled charge-coupled device (CCD) detector at room temperature, using the 514.5 nm Ar ion and 325 nm HeCd laser lines as excitation sources. The structures were investigated with a Hitachi H-8000 transmission electron microscope (TEM), an AutoProb CP atomic force microscope (AFM), and Cu $K\alpha$ radiation ($\lambda = 0.154\,18$ nm) x-ray diffraction (XRD) at room temperature.

For comparison, we also used the electrochemical etching method to disperse porous Si into nanocrystals. A *p*-type Si(100) wafer with a resistivity of 5–10Ω cm was laterally anodized in a 1:1:2 mixture of hydrofluoric acid (HF):H_2O:ethanol. Ethanol served to improve the wetting of the Si/porous-Si interface as well as to minimize hydrogen bubble formation. The Si wafer anode and platinum cathode were vertically immersed in the solution with an etching current of 40 mA/cm^2. After 12 min etching and several cycles of washing in diluted HF and deionized (DI) water, the porous Si layer shows visible yellow/orange light under the light of a hand-held UV lamp. A 10 min ultrasonic bath in DI water was applied to crumble the porous Si layer into nanocrystals. The suspension colloid of nanocrystals was then condensed and transferred onto Si(100) substrates, forming a uniform nanocrystal layer with crystal size less than 10 nm.

III. RESULTS AND DISCUSSION

A. Surface morphology and composition

We deposited Si nanocrystals in Ar and O_2 at different pressures. Figure 2 shows the surface morphology of Si nanocrystals deposited in Ar observed by scanning electron microscopy (SEM). With increasing Ar pressure, there is a transition from a film structure to a porous cauliflowerlike structure. As shown in Fig. 2(a), at a gas pressure of 1 mTorr, the SEM image shows a uniform background film as well as a big particle. The big particle is a macroscopic droplet of target material that is deposited on the substrates along with the film, which is a major drawback of PLD. As shown in Fig. 2(b), at a gas pressure of 100 mTorr, a film with undulating periodic crests and troughs is obtained. Figure 2(c) shows the image of Si nanocrystals deposited in 1 Torr. As shown in the left part of Fig. 2(c), separate crystals are deposited on the surface. They seem to agglomerate together, forming a porous cauliflowerlike structure. In the enlarged image in the right part of Fig. 2(c), crystals with an average size of 10 nm can be observed. However, such crystals may be composed of much smaller crystals.

The size distribution of Si nanocrystals deposited at different gas pressure can be explained by collisions between the ejected species. An increase of gas pressure will result in increasing collisions between the ejected species and the ambient gas. At a pressure of 1 mTorr, the mean free path of the ejected species is approximately 5 cm.[17] With our target-to-substrate distance of 6 cm, this means that there are only 1.2 collisions between the ejected species before they reach the

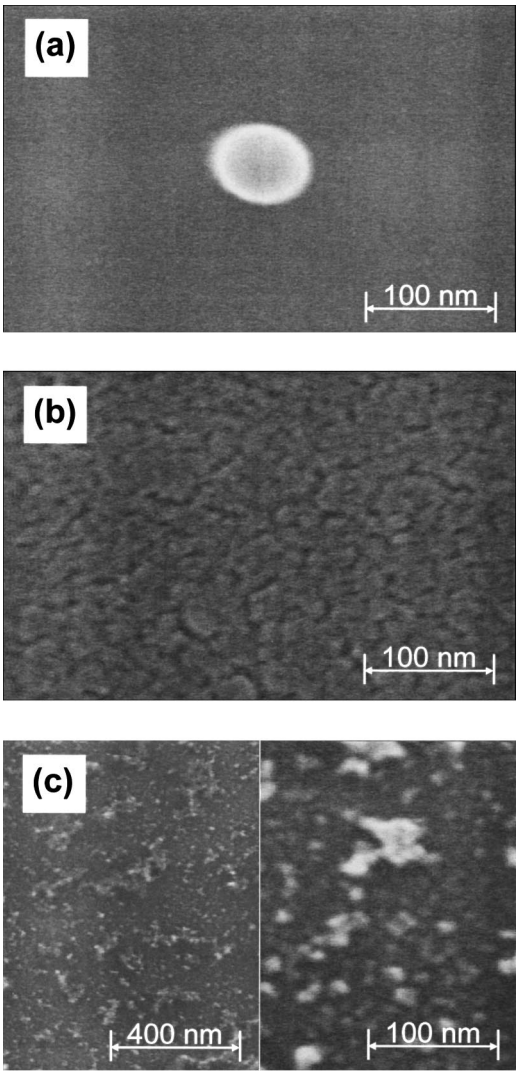

FIG. 2. SEM images of Si nanocrystals deposited in Ar at a pressure of (a) 1 mTorr, (b) 100 mTorr, and (c) 1 Torr.

substrate. As a result, solidified liquid droplets expelled from the target are predominant, while the vapor species are deposited as a background film. When the gas pressure increases, more collisions occur. The mean free path of the ejected species is 0.05 cm at a higher pressure of 100 mTorr.[17] The vapor species can undergo sufficient collisions to form small crystals, and thus nucleation and growth take place while the Si plasma plume expands toward the substrates. On the other hand, the arrival of the liquid droplets at the substrates is hampered by the increased collisions and gas pressure. Using gated intensified CCD-array imaging, Geohegan *et al.*[18] confirmed that 1 Torr Ar stops and reflects the Si plasma plume, resulting in a stationary, uniformly distributed nanocrystal cloud. Nanocrystals are unambiguously formed in the gas phase. Therefore, it can be concluded that the size distribution of the Si nanocrystals is greatly influenced by the ambient gas pressure.

The surface morphology of Si nanocrystals deposited in O_2 was also observed by SEM. A similar transition of surface morphology from a film structure to a porous cauliflowerlike structure is found in O_2 pressure from 1 mTorr to 1 Torr. The

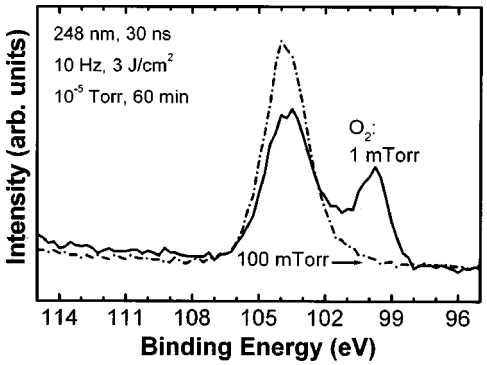

FIG. 3. Si $2p$ spectra of Si nanocrystal films deposited in 1 and 100 mTorr O_2 examined by XPS.

transition has also been reported by PLD of Si nanocrystals in helium pressure from 2.5 to 5.0 Torr.[19] We think that the variation of transition pressure in different gases is mainly due to the different atomic or molecular mass of the ambient gases. The mass ratio between the Si plasma plume and ambient gas atoms (Ar, He) has a major effect on the plume dynamics in the 0–1 Torr pressure range.[20] The heavier gas has a larger scattering energy to stop the ejected species. Ar atoms ($m=40$) effectively remove Si atoms ($m=28$) from the forward-expanding plasma flux and can even scatter them backward, while lighter He atoms ($m=4$) gradually slow down Si atoms by small-angle collisions.[20]

The ambient gas plays a crucial role in the formation of Si nanocrystals. The inert Ar gas only cools down the ejected species. On the other hand, the reactive O_2 gas reacts with the ejected species, consuming Si and forming an oxide shell around the Si nanocrystals (a smaller crystal size). The crystals are embedded in the Si oxide layer. The Si oxide films are principally composed of Si nanocrystals surrounded by a dense crystalline phase of SiO_2, all immersed in as amorphous (a-)SiO_2 matrix.[21] The oxygen content increases with increasing O_2 pressure until finally nearly stoichiometric SiO_2 is obtained.

The composition of the Si nanocrystal films was examined by XPS. Figure 3 shows the Si $2p$ spectra of Si nanocrystal films deposited in 1 and 100 mTorr O_2. For the film deposited in 1 mTorr O_2, a peak of elemental Si (Si^0) at a binding energy of 99.8 eV and a peak of Si bonding to oxygen (Si^{4+}) at 103.5 eV (Ref. 22) can be observed. When the O_2 pressure increases to 100 mTorr, the elemental Si peak is no longer found and the Si^{4+} peak becomes stronger and shifts to 104.0 eV, which corresponds to SiO_2.[22] Further XPS data analysis confirms that nearly SiO_2 stoichiometry is obtained at 100 mTorr O_2. Thus, it can be concluded that nearly SiO_2 is obtained above the O_2 pressure of 100 mTorr.

B. Photoluminescence spectra

The PL of Si nanocrystals deposited in Ar at different pressures was measured using two excitation sources. During the measurements, particular attention was paid to keep the excitation power at a constant level. The PL spectra at long wavelength using the Ar ion laser line as excitation source are presented in Fig. 4(a). A broad main peak is observed in

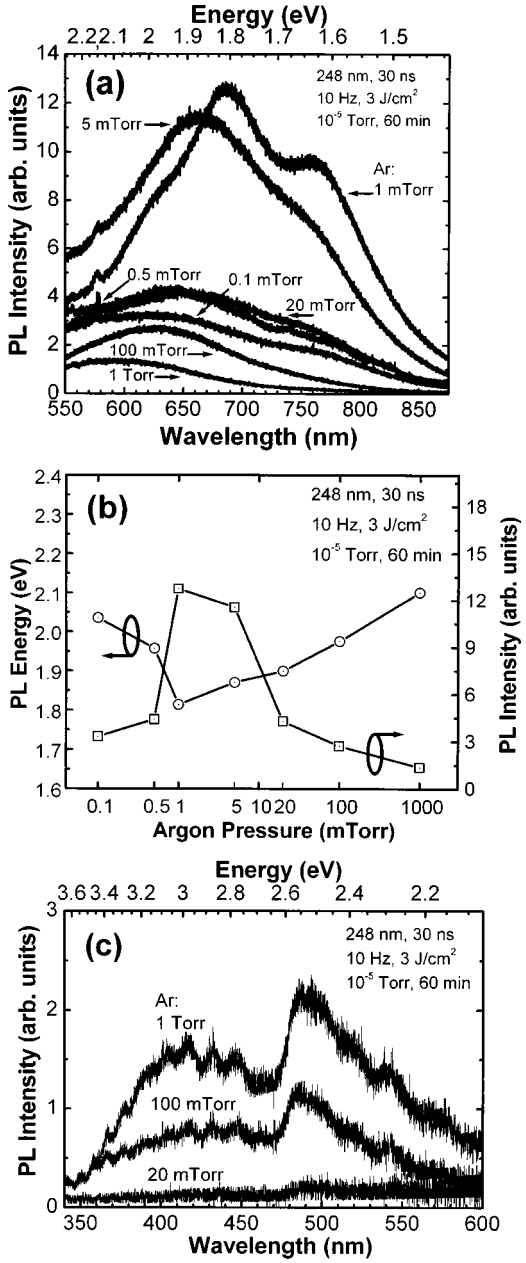

FIG. 4. PL spectra of Si nanocrystals deposited in Ar at different pressures. (a) The long wavelength range. (b) The peak position and intensity as a function of Ar pressure in (a). (c) The short wavelength range.

all samples. There is also a small shoulder for the sample deposited in 1 mTorr Ar, which corresponds to 1.64 eV. The PL spectra are highly dependent on the Ar pressure. For better illustration, the peak position and intensity as a function of Ar pressure are shown in Fig. 4(b). It is found that, with the increase of gas pressure from 0.1 to 1 mTorr, the peak is redshifted from 2.03 to 1.81 eV, while the PL intensity increases. Further increase of gas pressure from 1 mTorr to 1 Torr leads to a blueshift of the peak position from 1.81 to 2.10 eV and a decrease of PL intensity. At 1 mTorr Ar, there is a turnaround of the PL band shift and PL intensity. Figure 4(c) shows the PL spectra at short wavelength using the He-Cd laser line as excitation source. One single peak at 490 nm is observed in this range, which corresponds to 2.55 eV. The intensity increases with increasing Ar pressure while there is no shift in peak position. It is also found that the samples deposited below 20 mTorr Ar show similar spectra to that deposited in 20 mTorr Ar, with a weak intensity PL peak at 2.55 eV. (They are not shown in the figure.)

There has been a continuing controversy concerning the physical mechanisms for the light emission from Si nanostructures. Some work suggests that surface states and surface alloys are the principal mechanisms leading to PL.[23] There is also experimental evidence that amorphous species *a*-Si or *a*-SiO_x ($0<x\leqslant 2$) used to confine Si nanocrystals can be responsible for PL.[24] The present most commonly accepted theory is the quantum confinement effect (QCE), which can explain the PL properties behind many experimental data.[25] In the QCE theory, visible PL can be observed when the separation of the Si band gap is large enough due to the shrinkage or size reduction of the Si clusters. The high light emission efficiency results from high radiative recombination due to the quantum confined *c*-Si nanocrystals, whose surface is very well passivated by Si-H or Si-O bonds.

From Figs. 4(a) and 4(b), it is clear that the PL band at 1.8–2.1 eV is highly dependent on the ambient gas pressure. Different gas pressures result in size variation of the Si nanocrystals in the films as well as different surface morphologies (different microstructures), which might be responsible for the PL band shift at 1.8–2.1 eV. Thus, we assume that the PL band at 1.8–2.1 eV is attributed to the QCE in the Si nanocrystal core.

We also studied the dependence of the PL band at 1.8–2.1 eV on the distance between the measuring point and the center axis of the Si plasma plume. It is found that the PL band is blueshifted when the distance increases from 0 to 15 mm. The blueshift is around 0.05 eV at 1 mTorr Ar and increases to 0.15 eV at 1 Torr, since the scattering effect by the ambient gas is more pronounced at a higher gas pressure. Patrone *et al.*[16] reported that, with increasing distance from the ablation spot from 2 to 10 mm, the PL band shifts significantly to the blue from 2.0 to 2.4 eV, due to the size decrease of the Si nanocrystals. Thus, such a distance- or size-dependent PL clearly demonstrates the scattering of clusters in the Si plasma plume and confirms the QCE in Si nanocrystal cores.

In Fig. 4(c), the PL band at 2.55 eV is apparent only at high Ar pressure and the peak positions are fixed. The origin of this band can be explained by the light emission mechanism from the localized surface states at the SiO_x/Si interface. As the Si surface has a high affinity for O_2, an oxide layer rapidly forms when Si is exposed to an oxidizing ambient. Although small Si clusters have been measured to be about two orders of magnitude less reactive than a bare Si surface,[26] the environment in the ablated Si plasma plume appears to be more reactive.[18] Si can easily react with residual O_2 in the chamber and O_2 impurities in the Ar gas. Gas flow is essential to bring fresh oxygen-containing molecules into the vicinity of the stationary Si/Ar plume, forming silicon-rich silicon oxide nanocrystals.[18] For example, Geohegan *et al.*[27] found that $SiO_{1.4}$ stoichiometry is formed in 1 Torr Ar (99.9995%) gas flow. At higher gas pressure, the higher gas flow delivers more oxygen-containing molecules, which causes more oxidation. Furthermore, oxidation oc-

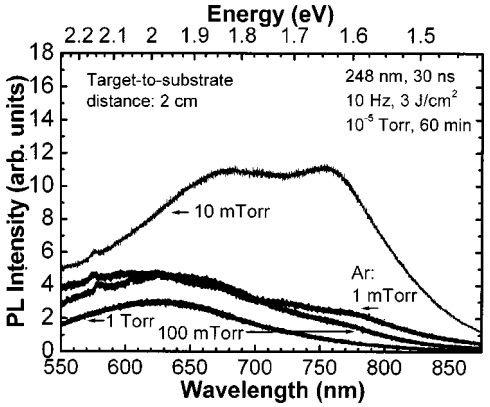

FIG. 5. PL spectra of Si nanocrystals deposited in Ar at a target-to-substrate distance of 2 cm.

curred as the samples were exposed in air before the PL measurements. From the SEM images, the porosity of the surface area of the as-deposited Si nanocrystals increases with increasing Ar pressure. Higher porosity will lead to stronger oxidation in air. The oxidation introduced localized surface states at SiO_x/Si interface. As a result, the intensity of the PL band at 2.55 eV increases with increasing Ar pressure.

Another reason for the origin of the PL band at 2.55 eV is that there are vibronic structures with periodic spacing of 97 ± 9 meV on the PL band at 2.55 eV. The vibronic structures are independent of experimental conditions, suggesting a strong surface characteristic of the structures. Kimura and Iwasaki[28] reported similar vibronic structures in the ultraviolet-visible PL band from Si nanocrystals with sizes of 3.7 and 6.2 nm suspended in organic solution. Progression analyses of these structures and IR spectra show that the structures come from various local vibrational modes that couple with the localized electronic state of surface chemical species related to oxygen. Kimura and Iwasaki concluded that the vibronic fine structures originate from a localized surface state of Si-O-Si or other modes. Thus, the most likely explanation for the PL band at 2.55 eV is localized surface states at the SiO_x/Si interface.

To understand the influence of collisions among the ejected species on the PL spectra, we used a smaller target-to-substrate distance of 2 cm in the deposition to observe the PL spectra. The results are shown in Fig. 5. It is found that the maximal PL intensity is obtained at 10 mTorr Ar. The PL spectrum of the sample deposited in 10 mTorr Ar is similar to that deposited in 1 mTorr Ar in Fig. 4(a). The turnaround of the PL band shift and PL intensity happens at 10 mTorr Ar. This pressure is higher than the 1 mTorr Ar when the target-to-substrate distance is 6 cm. As a small target-to-substrate distance greatly reduces the cooling time and the total number of the collisions between the ejected species, it has a similar effect as the decrease of gas pressure. Qualitatively, the deposition with a small target-to-substrate distance and high gas pressure is comparable to that with a large target-to-substrate distance and low gas pressure. Thus, the turnaround point of PL band shift and PL intensity shifts to higher gas pressure with decreasing target-to-substrate distance, which further confirms the great influence of species collisions on Si nanocrystal formation.

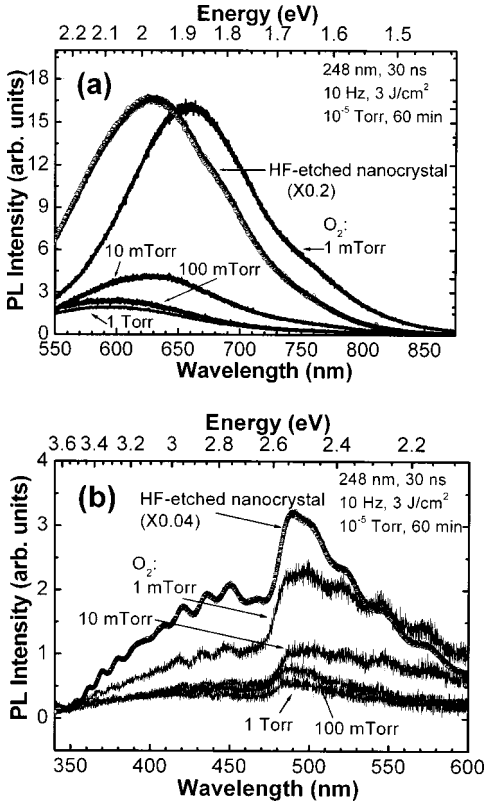

FIG. 6. PL spectra of Si nanocrystals deposited in O_2 at different pressures. (a) The long and (b) the short wavelength range.

Figure 6 shows the PL spectra of Si nanocrystals deposited in O_2. For comparison, the PL spectrum of the Si nanocrystal layer formed by the electrochemical HF etching method is also presented. As shown in Fig. 6(a), with the increase of O_2 pressure from 1 mTorr to 1 Torr, the peak is blueshifted from 1.87 to 2.12 eV with decreasing PL intensity. Compared with Fig. 4(a), the PL intensity deposited in 1 mTorr O_2 is around 1.3 times that deposited in 1 mTorr Ar. The intensity change and peak shift of PL spectra deposited in O_2 coincide with those deposited in Ar. Since the Si nanocrystals deposited in Ar and O_2 also have similar surface morphology, we believe that the PL band in Fig. 6(a) is still related to the QCE in the Si nanocrystal core. For the HF-etched nanocrystal PL spectrum, a single peak at 1.98 eV is observed with an intensity about five times that from Si nanocrystals deposited by PLD. The high PL density is due to the high crystal density of the Si nanocrystal layer. The PL spectrum is similar to that from Si nanocrystals formed by PLD in Ar and O_2. The light emission also agrees with the visible yellow/orange light of the porous Si layer. All the consistency among results support that the yellow/orange light emission of the PLD films as well as of the porous Si layer comes from the Si nanocrystal core.

As shown in Fig. 6(b), there are still the same single peak at 2.55 eV and vibronic structures with the same periodic spacing on the PL bands as those deposited in Ar in Fig. 4(c). For the Si nanocrystals deposited in O_2, the intensity decreases with increasing O_2 pressure while there is no shift

in peak position. From the XPS analysis, it is known that the oxygen content in the Si nanocrystal films increases with increasing O_2 pressure and nearly stoichiometric SiO_2 is formed at pressures higher than 100 mTorr. The localized surface states at the SiO_x/Si interface are reduced with increasing O_2 pressure. Therefore, the PL intensity decreases with increasing O_2 pressure. For the HF-etched nanocrystal PL spectrum, the intensity of the peak at 2.55 eV is about 40 times that from Si nanocrystals deposited by PLD, while the vibronic structures can be observed more clearly. The native oxide that confines the Si nanocrystals introduces a large amount of interface or defect (surface) states, which might explain the intense PL. It is noticed that the single peak at 2.55 eV and the vibronic structures of the PL spectra are independent of the process conditions (Ar or O_2) and the fabrication method (PLD or electrochemical etching), which strongly supports our conclusion that the PL band at 2.55 eV is a surface characteristic of Si nanocrystals.

C. Effects of oxidation and annealing

We applied oxidation and N_2 annealing to the as-deposited Si nanocrystals. The oxidation rate of Si is mainly dependent on the oxidation temperature and increases with increasing temperature. For bulk Si, the oxidation occurs at the Si/SiO_2 interface, which moves into the bulk Si by oxygen diffusion through the oxide.[29] For Si nanocrystals, on the other hand, oxidation is a well known self-limiting process.[30] The stress in the oxide layer that confines the Si nanocrystals can suppress the oxidation of Si nanocrystals, leading to a decreasing oxidation rate with decreasing crystal size. The oxidation rate is reduced to 1/3 for Si nanocrystals with an initial size of 15 nm compared with that of a Si(100) substrate for 15 h oxidation at 750 °C.[31] Complete oxidation of Si nanocrystals is difficult and Si nanocrystals are embedded in the oxide layer after oxidation. Oxidation can reduce the size of the nanocrystals (give rise to the QCE), convert the outer layer material into Si oxide (introduce the Si-SiO_x interface or defects in the oxide layer), and create *c*-Si in an oxide shell (passivate the nanocrystal surface). Thus, the PL spectra will be affected by the three combined effects of oxidation. Annealing is another common thermal treatment to recover the crystal structure of films. As some oxygen is in the N_2 gas flow, slight oxidation occurs during annealing in N_2.

Figure 7 shows the PL spectra of Si nanocrystal films deposited in 1 mTorr Ar after oxidation or annealing. As shown in Fig. 7(a), the films show enhanced PL intensities after oxidation and annealing. The PL intensity increases with increasing oxidation temperature. The strongest PL intensity, 2.6 times stronger than that from the as-deposited film, is obtained after annealing. It can also be seen that there are blueshifts of the peak position compared with the as-deposited film. As Si nanocrystals were annealed and passivated in an oxide shell during oxidation, their size is reduced. The QCE increases the band gap of Si nanocrystals. Therefore, the blueshift is strong evidence of a light emission mechanism based on the QCE.[32] The blueshift is larger after 900 °C oxidation than after 700 °C oxidation, while the smallest shift is observed after annealing. Since the oxidation rate of Si at 900 °C is one order of magnitude higher than that at 700 °C, the size reduction of Si nanocrystals in the films is greater at higher oxidation temperature, leading to a larger blueshift. The small blueshift for the annealed film is due to slight oxidation. All these results give strong evidence that the PL band at 1.8–2.1 eV is due to the QCE in the Si nanocrystal core.

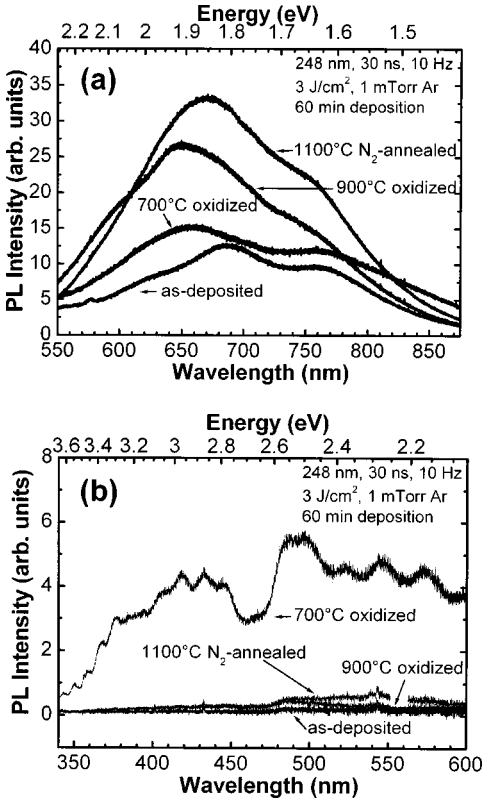

FIG. 7. PL spectra of Si nanocrystal films deposited in 1 mTorr Ar after oxidation or annealing. (a) The long and (b) the short wavelength range.

As shown in Fig. 7(b), only the Si nanocrystal film after 700 °C oxidation shows a significantly enhanced PL intensity with vibronic structures. For the film after 900 °C oxidation, the PL intensity is low, which is contrary to the enhanced PL intensity of the same sample measured in the long wavelength range in Fig. 7(a). In fact, PL from different layers was measured when we used two excitation sources. Due to the indirect nature of the Si band gap below 3.4 eV, the penetration depth of Ar ion laser light at 514.5 nm in *a*-Si and polysilicon ranges from 100 to 200 nm, while in *c*-Si it is about 500 nm. On the other hand, an excitation energy larger than 3.4 eV is above the direct E_1 transitions of Si, making the optical absorption coefficient much larger. At the He-Cd laser line of 325 nm (3.82 eV), the penetration depth ($1/\alpha$) in *c*-Si is 8 nm, where α is the optical absorption coefficient.[33] PL spectra with such high excitation energy will probe a much shallower region of Si. As a result, the PL spectra shown in Fig. 7(b) are dominated by the surface layer of the nanocrystal film while the PL spectra in Fig. 7(a) may come from the whole film, as the film thickness is around 100 nm measured by surface profiling. Due to the deeper oxidation of the surface layer, there is depth-dependent PL, which can

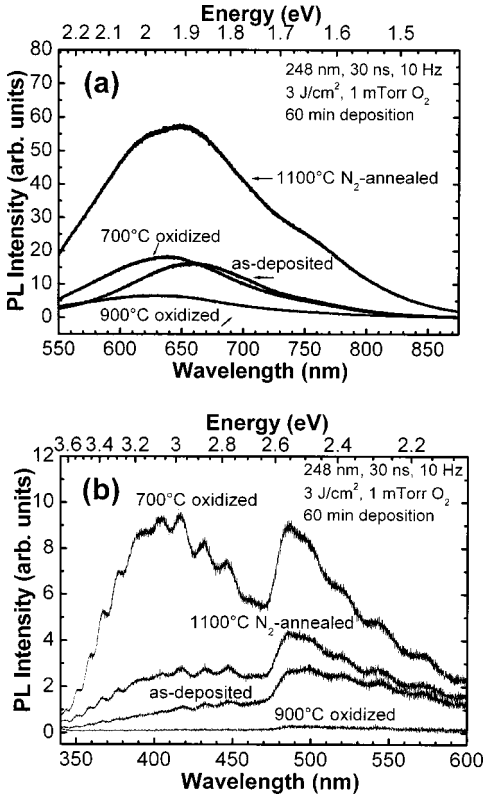

FIG. 8. PL spectra of Si nanocrystal films deposited in 1 mTorr O_2 after oxidation or annealing. (a) The long and (b) the short wavelength range.

explain the disagreement of the 900 °C oxidized film between Figs. 7(a) and 7(b). As to the annealing, localized surface states at the SiO_x/Si interface are slightly increased due to slight oxidation. Thus, the PL intensity at 2.55 eV slightly increases after annealing.

Figure 8 shows the PL spectra of Si nanocrystal films deposited in 1 mTorr O_2 after oxidation or annealing. As shown in Fig. 8(a), the films show decreased PL intensity after 900 °C oxidation but enhanced PL intensities after 700 °C oxidation and 1100 °C annealing. There is the same blueshift dependence on the thermal treatment as that in 1 mTorr Ar. However, the blueshift is much smaller. Since the film deposited in O_2 has a smaller crystal size and a large amount of oxygen, it can be oxidized more easily than the Si nanocrystal films deposited in Ar. High-temperature oxidation at 900 °C leads to strong oxidation of the film and thus a decrease of PL intensity. On the other hand, the oxidation of Si nanocrystals in the film is also more retarded due to the higher compressive stress from the outer oxide layer at a smaller crystal size, resulting in a smaller blueshift.

As shown in Fig. 8(b), the Si nanocrystal film shows a decreased PL intensity after 900 °C oxidation, which agrees with Fig. 8(a). The film after 700 °C oxidation displays another broad peak at 2.98–3.06 eV with vibronic structures, which was also reported by Geohegan *et al.*[27] They suggested that their broad vibronic PL band at 3.2 eV is due to photoexcitation of Si-Si vibrations at localized surface states, which is a surface characteristic of Si nanostructures. From our PL spectra evolution, it can be seen that the PL peak at 2.98–3.06 eV shows good correlation with the PL peak at

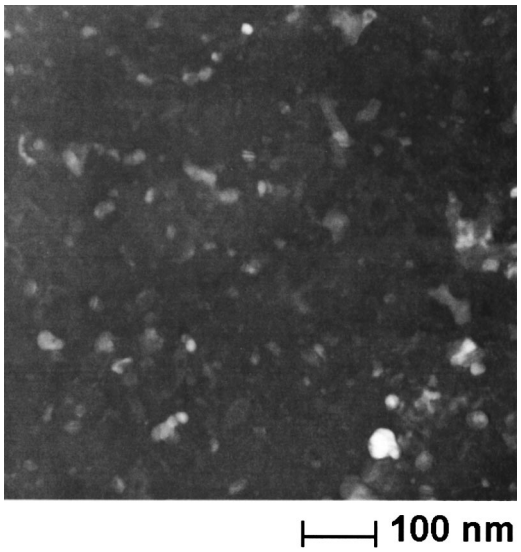

FIG. 9. Planar-view TEM image of Si nanocrystal film deposited in 1 mTorr Ar.

2.55 eV. Thus, we believe that the PL peak at 2.98–3.06 eV is still related to the localized surface states at the SiO_x/Si interface.

D. Crystal structure

TEM was carried out to characterize the crystal structure of the films. The planar-view TEM image of the Si nanocrystal film deposited in 1 mTorr Ar is shown in Fig. 9. It reveals a structure composed of a large number of very fine Si nanocrystals with an average size of about 10 nm. To get a better understanding of the crystal structure, we used atomic force microscopy (AFM) to further characterize the size distribution of the Si nanocrystals. As the Si nanocrystals were formed in a gas ambient in the PLD process, the properties of the substrate surfaces were degraded. A fraction of a monolayer of clusters was deposited on a highly oriented pyrolitic graphite (HOPG) substrate, using the same experimental conditions (Ar gas pressure 1 mTorr, laser fluence 3 J/cm^2). The HOPG has an atomically flat surface suitable for reliable AFM measurements at the nanoscale. It is known that the real sizes of nanoclusters are truly represented by the height values from AFM measurements, while their lateral dimensions are usually enlarged due to the tip-particle convolution effect. Thus, the height values were taken to be the crystal sizes. A wide distribution of crystal size ranging from 1 to 20 nm was obtained, with two size peaks at around 2.5 and 10 nm. We believe that the AFM measurement is more accurate since it can detect smaller crystal sizes and is not affected by the agglomeration of the crystals. Theoretical calculations[34] and experimental data[16,35] have consistently shown that the optical band gap ranges from 1.6 to 2.3 eV for Si nanocrystals with an average size between 5.0 and 2.5 nm. Although our mean crystal size is slightly larger compared with that associated with the QCE-induced PL spectrum obtained at 1.8–2.1 eV, it is believed that the PL band arises from the smaller nanocrystals in the size distribution and originates from Si nanocrystals with sizes between 5 and 1

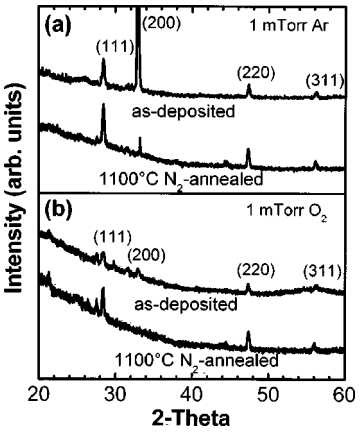

FIG. 10. XRD spectra of Si nanocrystal films deposited in 1 mTorr (a) Ar and (b) O_2.

nm. From the TEM and AFM results, the size of the Si nanocrystals is not uniform. As mentioned above, the properties of the deposited species are largely determined by the collisions between the ejected species. The nonuniformity is due to few collisions at 1 mTorr Ar.

We also used Raman shift to estimate the crystal size in the films. The Raman scattering spectra were obtained using the 514.5 nm Ar ion laser line as excitation source. The Raman peak position measured from the *c*-Si substrate is 520.3 cm^{-1}, while the full width at half maximum (FWHM) is 4 cm^{-1}. For the film deposited in 1 mTorr Ar, the Raman peak shifts to 518.2 cm^{-1}, while the FWHM is 6 cm^{-1}. According to the phonon confinement model given by Campbell and Fauchet,[36] the phonon confinement effects cause a shift of the Raman spectrum to lower wave numbers since the crystal size decreases, while the width of the Raman spectrum is correlated with the size distribution of the crystals. Using the model, the crystal size by the Raman shift 2.1 cm^{-1} and FWHM 6 cm^{-1} is calculated to be around 9 nm, which is in agreement with the TEM result. However, it should be pointed out that, during the estimation, the interference in the Raman line from the *c*-Si substrate was not taken into account, although it is always strong. The agglomeration of Si nanocrystals may also increase the size of the phonon confinement region.

Figure 10 shows the XRD spectra of Si nanocrystal films deposited in Ar and O_2. It is found that the XRD spectra of the films exhibit peaks typical for *c*-Si. The peak (200) comes from the *c*-Si substrate. The multipeak of the as-deposited films reveals a polysilicon structure. All the films show enhanced diffraction peaks after annealing, which indicates a better crystallinity. In the PLD process, the species in the Si plasma plume ejected by laser ablation are cooled down and stabilized by the ambient gas, a process which starts about 50–100 ns after the laser pulse. Condensation of vapor during the fast expansion of the plume occurs in strongly nonequilibrium conditions. The characteristic cooling rate for the plume expanding into vacuum reaches 10^{10}–10^{11} K/s. Le *et al.*[11] reported that in 5–100 μs after the ablation pulse, the SiO temperature decreases from around 2300 to 500 K in 100 mTorr Ar. Due to the lack of kinetic energy, all the impinging nanocrystals essentially stick to the substrates. The separated nanocrystals may attract each other, forming an agglomeration. As a consequence of the rapid cooling, Si nanocrystals with metastable structure (i.e., an amorphouslike structure) can be formed. Makino *et al.*[12] found that as-deposited Si nanocrystals show poor crystallinity. After annealing, many Si nanocrystalline cores are observed and the crystallinity of Si nanocrystals is recovered. Therefore, subsequent annealing of as-deposited Si nanocrystals is necessary for a more stable structure and better crystallinity.

IV. CONCLUSIONS

Si nanocrystals have been formed by PLD in Ar and O_2 gases. Oxidation and annealing were applied to the Si nanocrystals. The as-deposited Si nanocrystals show a transition from a film structure to a porous cauliflowerlike structure with increasing ambient gas pressure, due to the collisions between the ejected species. The oxygen content of Si nanocrystals increases with increasing ambient pressure and nearly SiO_2 stoichiometry is obtained at higher O_2 pressure. PL peaks at 1.8–2.1 and 2.55 eV were found from the Si nanocrystals. The peak shifts with ambient gas pressure and blueshifts after oxidation and annealing support the conclusion that the PL band at 1.8–2.1 eV is due to the QCE in the Si nanocrystal core. The periodic vibronic structures and no peak shift relate the PL band at 2.55 eV to the localized surface states at the SiO_x/Si interface. PL spectra of Si nanocrystals obtained by crumbling an electrochemically etched porous Si layer further confirmed our conclusion. Raman and TEM results provided a consistent crystal size while more accurate AFM measurements showed a smaller crystal size. XRD reveals that the as-deposited Si nanocrystals have a polycrystal structure. Subsequent annealing is necessary for a more stable structure and better crystallinity.

ACKNOWLEDGMENTS

The authors would like to acknowledge the help of H. L. Koh and C. H. Soh with technical support.

[1] S. Furukawa and T. Miyasato, Jpn. J. Appl. Phys., Part 2 **27**, L2207 (1988).
[2] H. Takagi, H. Ogawa, Y. Yamazaki, A. Ishizaki, and T. Nakagiri, Appl. Phys. Lett. **56**, 2379 (1990).
[3] L. T. Canham, Appl. Phys. Lett. **57**, 1046 (1990).
[4] H. I. Hanafi, S. Tiwari, and I. Khan, IEEE Trans. Electron Devices **43**, 1553 (1996).
[5] L. Guo, E. Leobandung, and S. Y. Chou, Appl. Phys. Lett. **70**, 850 (1997).
[6] M. Ehbrecht, H. Ferkel, F. Huisken, L. Holz, Y. N. Polivanov, V. V. Smirnov, O. M. Stelmakh, and R. Schmidt, Appl. Phys. Lett. **78**, 5302 (1995).
[7] T. S. Iwayama, S. Nakao, and K. Saitoh, Appl. Phys. Lett. **65**, 1814 (1994).
[8] L. S. Liao, X. M. Bao, X. Q. Zheng, N. S. Li, and N. B. Min, Appl. Phys. Lett. **68**, 850 (1996).
[9] K. H. Jung, S. Shih, T. Y. Hsieh, D. L. Kwong, and T. L. Lin, Appl. Phys. Lett. **59**, 3264 (1991).
[10] G. Belomoin, J. Therrien, A. Smith, S. Rao, R. Twesten, S. Chaieb, M. H. Nayfeh, L. Wagner, and L. Mitas, Appl. Phys. Lett. **80**, 841 (2002).
[11] H. C. Le, R. W. Dreyfus, W. Marine, M. Sentis, and I. A. Movtchan, Appl. Surf. Sci. **96-98**, 164 (1996).
[12] T. Makino, Y. Yamada, N. Suzuki, T. Yoshida, and S. Onari, J. Appl. Phys. **90**, 5075 (2001).

[13] T. Yoshida, S. Takeyama, Y. Yamada, and K. Mutoh, Appl. Phys. Lett. **68**, 1772 (1996).
[14] N. Suzuki, T. Makino, Y. Yamada, T. Yoshida, and T. Seto, Appl. Phys. Lett. **78**, 2043 (2001).
[15] A. V. Kabashin, J.-P. Sylvestre, S. Patskovsky, and M. Meunier, J. Appl. Phys. **91**, 3248 (2002).
[16] L. Patrone, D. Nelson, V. I. Safarov, M. Sentis, and W. Marine, J. Appl. Phys. **87**, 3829 (2000).
[17] L. Y. Chen, in *Pulsed Laser Deposition of Thin Films*, edited by D. B. Chrisey and G. K. Hubler (Wiley, New York, 1994), p. 186.
[18] D. B. Geohegan, A. A. Puretzky, G. Duscher, and S. J. Pennycook, Appl. Phys. Lett. **72**, 2987 (1998).
[19] N. Suzuki, T. Makino, Y. Yamada, T. Yoshida, and S. Onari, Appl. Phys. Lett. **76**, 1389 (2000).
[20] R. F. Wood, K. R. Chen, J. N. Leboeuf, A. A. Puretzky, and D. B. Geohegan, Phys. Rev. Lett. **79**, 1571 (1997).
[21] I. A. Movtchan, R. W. Dreyfus, W. Marine, M. Sentis, M. Autric, G. Le Lay, and N. Merk, Thin Solid Films **255**, 286 (1995).
[22] F. G. Bell and L. Ley, Phys. Rev. B **37**, 8383 (1988).
[23] F. Koch, V. Petrova-Koch, and T. Muschik, J. Lumin. **57**, 271 (1993).
[24] S. M. Prokes, Appl. Phys. Lett. **62**, 3244 (1993).
[25] B. Delley and E. F. Steigmeier, Phys. Rev. B **47**, 1397 (1993).
[26] M. F. Jarrold, Science **252**, 1085 (1991).
[27] D. B. Geohegan, A. A. Puretzky, G. Duscher, and S. J. Pennycook, Appl. Phys. Lett. **73**, 438 (1998).
[28] K. Kimura and S. Iwasaki, Jpn. J. Appl. Phys., Part 1 **38**, 609 (1999).
[29] L. E. Katz, in *VLSI Technology*, edited by S. M. Sze (McGraw-Hill, New York, 1988), p. 99.
[30] D. B. Kao, J. P. McVittie, W. D. Nix, and K. C. Saraswat, IEEE Trans. Electron Devices **ED-35**, 25 (1988).
[31] J. Omachi, R. Nakamura, K. Nishiguchi, and S. Oda, Mater. Res. Soc. Symp. Proc. **638**, F531 (2001).
[32] P. M. Fauchet, J. Lumin. **70**, 294 (1996).
[33] D. E. Aspnes and A. A. Studna, Phys. Rev. B **27**, 985 (1983).
[34] C. Delerue, G. Allan, and M. Lannoo, Phys. Rev. B **48**, 11 024 (1993).
[35] G. Ledoux, O. Guillois, D. Porterat, C. Reynaud, F. Huisken, B. Kohn, and V. Paillard, Phys. Rev. B **62**, 15 942 (2000).
[36] T. I. Campbell and P. Fauchet, Solid State Commun. **58**, 739 (1986).